Rotatable cam-based variable-ratio lever compliant actuator for wearable devices

Miha Dežman, Andrej Gams

Abstract

This paper presents a novel variable stiffness mechanism based on the combination of a rotatable cam and a variable-ratio lever principle. The proposed configuration results in i) a pseudo-linear torque/deflection characteristics, where ii) the stiffness is varied rotationally and perpendicularly to the external load. The first is convenient for easier mechanism dimensioning and offers a more conventional control design. The second allows for a more energy efficient stiffness variation, thereby enabling the use of a less powerful stiffness variation motor and a reduction of the overall actuator weight and size. The presented mathematical model derivation and theoretical evaluation support both desired mechanism characteristics. Practical use of the mechanism is evaluated through the application of the developed prototype in a fully sensorized variable stiffness actuator intended for a wearable application. The results of the experiments and a comparison to other variable stiffness mechanisms show that the mechanism geometry is convenient for light and compact design.

Keywords: variable stiffness, cam mechanism, variable-ratio lever, energy efficient, linear torque/deflection, fast stiffness variation

1. Introduction

Functionality and usefulness of robotic systems are making rapid progress. For example, wearable devices, such as exoskeletons, have progressed to the

^{*}Department of Automation, Biocybernetics and Robotics, Jožef Stefan Institute, Jamova 39, 1000 Ljubljana, Slovenia

^{**}Jozef Stefan International Postgraduate School, Jamova 39, 1000 Ljubljana, Slovenia *Email addresses:* miha.dezman@ijs.si (Miha Dežman), andrej.gams@ijs.si (Andrej Gams)

stage where they can efficiently provide assistance and even augment user performance [1]. While many advances rely on advanced control techniques [2, 3], the mechanical design has been just as important. This has been shown in the design of various robotic mechanisms, for example, in humanoid robots [4, 5, 6] and jumping robots [7], but also in the aforementioned wearable devices [8, 9, 10]. Aspects of mechanical design include the choice and properties of the actuators, which can critically determine the intended application of use.

Among the different actuators, mechanically compliant actuators meet many suitable performance criteria for force-oriented applications [11]. By taking advantage of elastic elements either in a series (series elastic actuator – SEA) or in a parallel configuration (parallel elastic actuator – PEA), increased speed or higher torque can be achieved [12]. Furthermore, utilizing elastic elements can lower the cost and weight of the drive units because it allows the use of smaller and lower precision components and allows the replacement of expensive load cells with a simple spring with position transducers [13]. The latter can even make force measurements less prone to chatter and noise. Higher impedance and higher stiction components in these type of actuators are not detrimental to such use [13].

While the SEA typically adopts a fixed-compliance elastic element, it can be controlled to render a variable compliance including nearly zero stiffness and a high stiffness up to the inherent mechanism stiffness [36]. The more advanced variable stiffness actuators (VSAs) use a second motor to add the ability of mechanical compliance adaptation. The secondary motor acts on the elastic element, for example through changing its strain [14], or the lever-length it acts on [15], to achieve different behavior. Through this, the VSAs can modulate their natural dynamics [16], or improve SEA power modulation. The latter was, for example, used to achieve greater vertical jumping ability [7] and efficiency [17]. VSA mechanisms can also adapt the stiffness to achieve different assistance levels in rehabilitation tasks based on the progress of the patient [18]. Having two motors and a mechanical system to change the stiffness parameters increases the geometrical complexity of VSA devices, and also makes them heavier and more expensive. However, this also creates the opportunity for simplifications and cost reduction [19] through the mechanical design.

This paper:

- proposes a novel VSA actuator principle with a convenient rotational geometry and potential for future compact units,
- shows the derivation and analyzes its mathematical model,
- presents a prototype drive unit implementing the proposed principle,
- shows the use of the prototype unit to evaluate the mathematical model, its

advantages and disadvantages, and

- compares it to other actuators that are most relevant to this work.

The intended application of the proposed mechanism is the actuation of wearable devices, more specifically, a 1 DoF elbow exoskeleton. However, the focus of this paper is on the compliant actuator, and not on the exoskeleton device.

The basic concept of rotational stiffness variation was previously presented and tested with a plastic prototype in a proof of concept [35]. However, it was not appropriate for application use due to a higher mechanical complexity. In this work, the number and diversity, including the mechanical complexity of different mechanical components, were all reduced. The device was made ready for practical applications and was thoroughly evaluated.

The rest of the paper is organized as follows. In the next Section, a short literature review and highlights of the desired VSA actuator are presented. In Section 3, the proposed operational principle of the mechanism, and the derivation and evaluation of its mathematical model, are presented. Section 4 describes the experimental setup with results shown in Section 5. In Section 6.1, the prototype is evaluated in light of other similar VSA actuators, ending with a discussion in Section 6.2. Finally, a conclusion follows in Section 7.

2. Related work

Research on compliance enabling devices has been very extensive. A broad overview of different compliance types, e.g., emulated active compliance, fixed inherent mechanical compliance (SEA) or actuators with mechanically varied compliance (VSA) and different technologies enabling it, is presented in [20]. In the following short overview, the focus lies on the compliant actuators with a mechanical variable stiffness, which represent only a fraction of available compliance enabling technologies.

The favorable properties enabled by mechanical compliance, and the endless possibilities to implement elastic elements into the actuator geometry resulted in a vast amount of architecture structures and variants. The reader is referred to [21, 22, 23] for an in-depth review of architectures of such inherent compliance mechanisms.

One can exploit the advantages of both fixed compliance actuators (SEAs) and variable stiffness actuators (VSAs). Considering a gait-assistance device, both SEA and VSA find suitable applications [24]. In many situations, using a VSA would provide only minimal benefits, while needlessly increasing the complexity and the weight. However, a suitable fixed compliance is often not immediately

clear, so in research situations, a variable stiffness device is advantageous, because it enables quick and practical stiffness adaptations. Overall, the VSAs are defined by a broader number of parameters than classical actuators or SEAs, e.g. the deflection range, stored energy, stiffness variation speed, etc. These variables are nicely presented in [25] and [26].

Besides design properties from the point of view of achieving variable stiffness, the VSAs are considered in the scope of wearable devices. Here, energy efficiency can mean a longer battery time. A lighter and smaller actuator can, furthermore, reduce the added weight impact and the amount of kinematic obstructions on the user. The suitability of such actuators is correlated with the desired application or task, which also makes the comparison between them difficult.

Three VSA actuator types have had a considerable influence on the field and the presented work. These are the MACCEPA-type VSAs, the DLR (German Aerospace Center) actuators, and the AwAS actuators. They have easily distinguishable operation principles and a high amount of available literature data. Many other VSA variants also exist [31, 32, 33, 34], but often use a larger amount of non-standard parts, which increases not only their complexity but also the complexity of their comparison.

The well established MACCEPA VSA principle [27] has a uniquely simple and straightforward way to vary the stiffness. Its compliance is achieved through a third link that deflects and pulls on a steel cable connected to a linear spring. The relative position of the external link to the third link determines the equilibrium position. To change the stiffness, a second motor can pretension the elastic element. Overall, the MACCEPA is known for a large deflection range and its ability to store a lot of elastic energy. Its flat and long structure makes it suitable for wearable applications, since it keeps the hardware close to the limbs, but also makes design of compacter units more difficult.

However, over the years, other versions of the MACCEPA VSA appeared. A pulley upgrade in MACCEPA 2.0 [39] enabled task-based modification of the actuators deflection characteristics. The use of extension springs in the WHEELED MACCEPA increased the actuators robustness and was later implemented in ALTACRO exoskeleton [38]. Recently, the use of a torsion spring in the TORSION MACCEPA version enabled a very compact actuator structure [37]. However, none of these versions tackled the difficulty of the pretension based stiffness variation system. Here, the force needed to change the pretension is applied in parallel to the load. The stiffness motor needs to additionally overcome the elastic-element load. The MACCEPA mechanism is thus suitable for less dynamic stiffness variation scenarios.

The Italian Institute of Technology (IIT) has presented AwAS-I [15] and AwAS-II [30] VSAs. In these, the deflection torque is generated when a lever arm compresses a linear spring. A screw mechanism can then linearly move the spring to change the lever length, which determines the torque required to compress the spring. A longer lever length results in a higher stiffness. Performance-wise, the AwAS has a distinct advantage, since in its mechanical architecture, it varies the stiffness perpendicularly to the spring load. Most of the load on the spring gets transfered through the mechanical structure of the actuator and not through the stiffness variation motor. The stiffness motor needs to overcome the friction in the bearings and inertia, only. This feature can be exploited either in favour of a faster stiffness variation or in a lower stiffness variation torque, and thus a less powerful stiffness variation motor.

On the other hand, the DLR actuator VS-Joint [28] and its second version DLR FSJ [14] have a very compact structure, enabled by the exploitation of the cam mechanism principle. The compactness was also demonstrated in the DLR Hand Arm System [29] implementation, where all joints are mechanically compliant. Here, the deflection is achieved via the rotation of a cam disk that compresses a spring-loaded follower. Higher stiffness is again achieved via spring pretension. While the cam mechanism offers a convenient way to transmit rotation motion into linear deflection, due to the pressure angle, the force transmission is less effective. Thus, the actuator implements a very stiff spring and needs large forces to generate a deflection torque comparable to other actuators. This imposes considerable constraints when the VSA actuator weight reduction and efficiency are prioritized, and is also why this is not preferred for an exoskeleton application. Consequently, the actuator structure needs to be stronger and very rigid to withstand the spring force, which increases the complexity and weight of the actuator. Considering a wearable application, the cylindrical shape is also not very convenient due to the volume extension along the joint axis.

The required features for the intended application include a fast and efficient stiffness variation, thus the pretension-less and perpendicular stiffness variation is advantageous. The actuator should allow the possibility of a compact design. The involved components should be easily manufacturable. Classical rotational bearings are preferred over linear ones. Overall, the goal is to design an actuator with a flat, light and efficient structure that will be suitable for a wearable application. In this paper, a novel VSA is proposed, called the Pseudo-linear Variable-ratio Lever Variable-Stiffness Actuator (PLVL-VSA), which combines these features.

3. Pseudo-linear Variable-ratio Lever Variable-Stiffness Actuator (PLVL-VSA)

This section presents the base operation principle of the proposed VSA. The internal mechanism, using a cam and a variable-ratio lever principle combination, is expanded to allow for bidirectional applications through a steel cable transmission, or the external mechanism. The presented derivation of the mathematical model allows the description of the torque/deflection characteristics, the torque required to hold stiffness and the amount of stored elastic energy, and therefore a theoretical evaluation of the device.

3.1. The operation principle and the internal/external mechanism

The proposed mechanism is shown in Fig. 1, featuring the flat-out mechanism drawings and the equivalent CAD drawings of the prototype. A VSA usually has

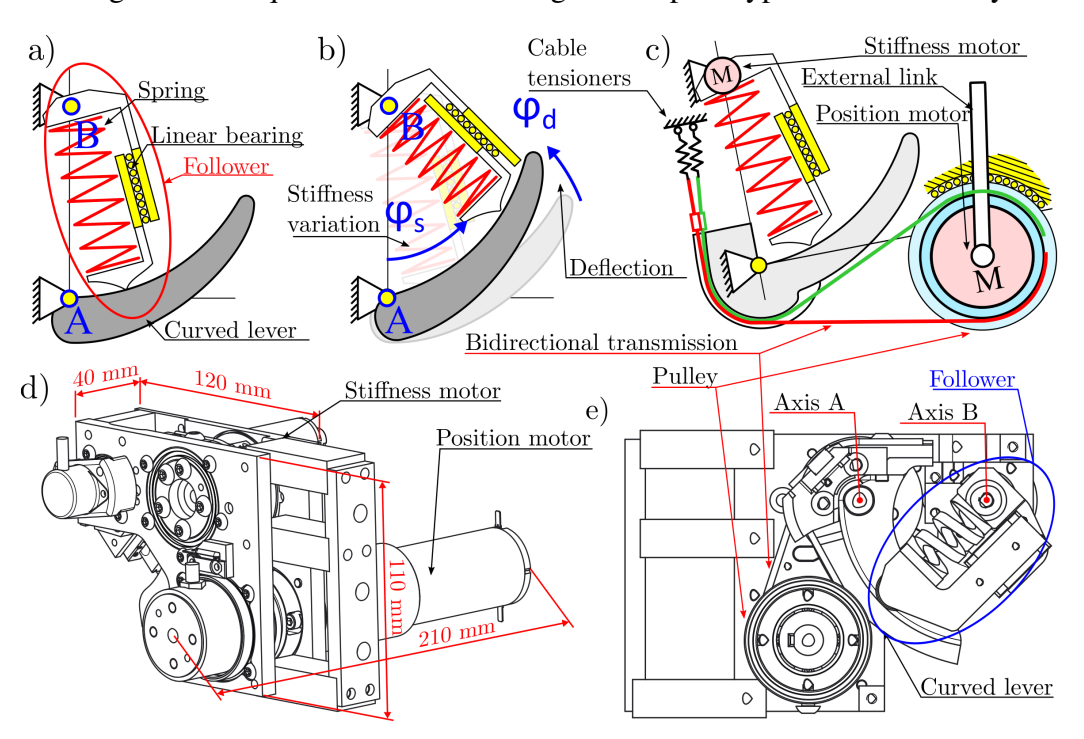


Figure 1: The flat-out representation of the internal mechanism components is shown in **a**). The compression movement is shown in **b**) with a marked cam follower angle (φ_s) and deflection angle (φ_d) . A more detailed depiction of the bidirectional VSA mechanism is shown in **c**). The CAD model of the VSA with dimensions is shown in **d**) with its internal view in **e**).

two motors. The first (hereafter called the *position motor*), usually a more powerful one, either supplies the desired torque or changes the systems equilibrium

position. The second motor can adapt the mechanism's stiffness (hereafter called the *stiffness motor*), and is usually a less powerful one.

As shown in Fig. 1(a), the mechanism combines the cam and variable-ratio lever principles. In base form, the lever arm connected to the external link rotates/deflects (φ_d) around pivot point A and compresses the spring. This provides a reaction torque to the external load. The follower (see Fig. 1(a)) can rotate around pivot point B to change the stiffness. The stiffness motor is located directly at pivot point B. To retain the desired stiffness, one can stop the stiffness motor at the appropriate angle – at an appropriate position of the follower on the lever arm. A higher cam follower angle (φ_s) produces a longer effective torque arm, resulting in a higher mechanism stiffness (see Fig. 1(b)). This makes up the basis of the proposed variable stiffness mechanism.

The lever arm has a circular arc shape, meaning that at zero deflection the radius between the pivot B and the contact at the curved shape is constant. Consequently, at zero deflection, the stiffness can be varied without resistance. Shapes deviating from a circular arc would either result in pretension of the mechanism or its slack. The stiffness is varied perpendicularly to the load, similarly to [15], and the majority of the stiffness-motor power is used to vary the stiffness. Therefore, the mechanism falls into the category of preloadless mechanisms [26] where the stiffness is varied by changing the transmission ratio. However, as the deflection angle increases, the follower is not completely perpendicular to the curved lever anymore, and thus a tangential force appears due to the change in the pressure angle. This needs to be accounted for in the design. The proposed principle, shown in Fig. 1(a) and 1(b) can support compression loads only. In this work, this part is marked as the *internal mechanism*.

A special transmission is needed to allow for a bidirectional application. One can use a cable transmission. Simplicity of implementation and reduction of the overall number of parts are two of its clear benefits. Other transmission types are possible for the same purpose, e. g. see [35]. Through the bidirectional deflection, the mechanism becomes a full-fledged VSA. In this work, this bidirectional mechanism is called the *external mechanism*. A depiction of the complete prototype actuator is presented in Fig. 1(d,e).

In the proposed setup (see Fig. 1(c)), the position motor housing is rigidly mounted onto a hollow pulley. The position motor axis passes through the hollow pulley and is fixed to the external link. The rotation of the position motor shaft directly influences the equilibrium position of the external link. The pulley-motor assembly can then rotate, and due to the cable transmission also deflect the curved lever, which rotates around pivot point A. The final implementation of the cable

transmission is explained in a detailed schematic depiction backed up with a CAD model in Fig. 2.

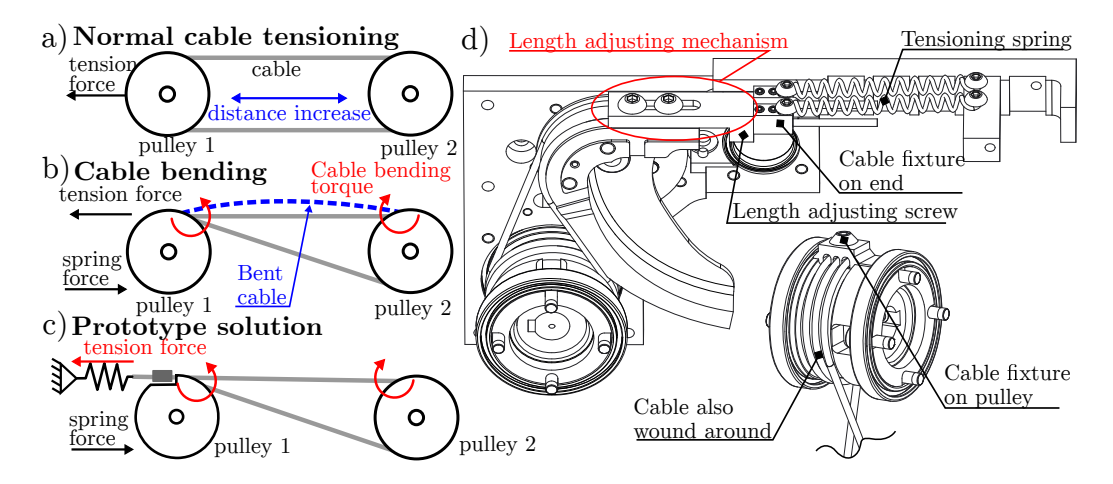


Figure 2: A classical cable transmission is tensioned through a distance increase between the pulleys, as shown in **a**). The prototype cable system is connected with both ends onto the same side of the pulley 1, see **b**). Classical tensioning is thus not possible and the internal bending torque in the cable also affects the mechanism load. The proposed tension solution is shown in **c**). The cable is tensioned through a spring connected to the mechanism housing. A CAD model representation of the actual prototype solution is shown in **d**).

To transfer the external torque through the cables, the cable is fixed at a pulley with a cable fixture (see Fig. 2(d)). The cable is routed around the pulley in both directions to provide additional friction and reduce the strain on the point fixture. On the other end, the cable is routed over the circular-arc lever, but fixed to the mechanism housing through an elastic element. The elastic element in between the housing and the cable provides the tension that alleviates the cable nonlinearity and ensures the cable does not lift off the pulley. The cable is also tensioned through a slight preload on the cam follower to additionally ensure that the follower does not lift off. It is presented later in Section 5.1. A blocking element mounted on the cable allows it to pull the curved lever. While this mechanism appears quite complicated, the manufacture of its parts is less complicated as the custom gears in previous work [35].

3.2. Mathematical model of the internal mechanism

Fig. 3 presents the main parameters affecting the basic model. R_s and R_b define the overall mechanism dimensions. Parameter R_b was added to account for

additional bearing space at pivot point A. The internal properties of the mechanism are defined through the elastic element stiffness k_{int} . The basic model does not account for the cable transmission and in that way effectively describes the internal mechanism only.

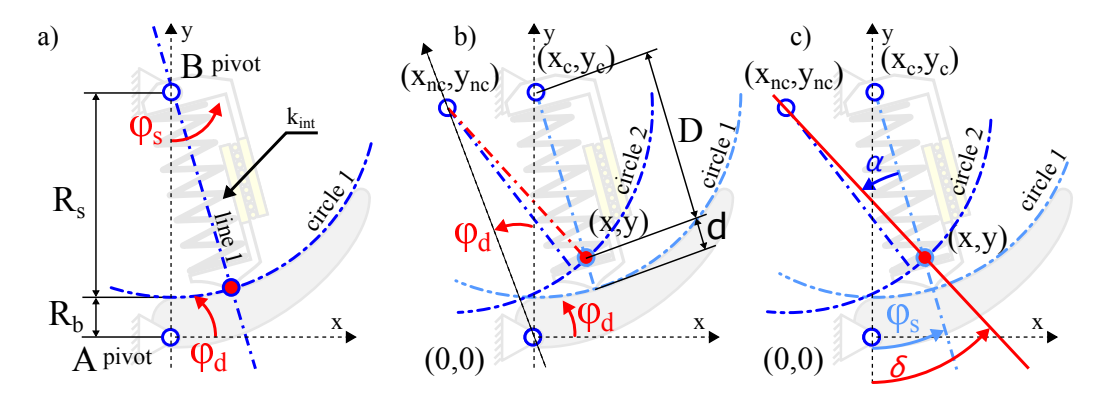


Figure 3: The flat-out simplified view of the proposed mechanism with its relevant parameters is shown in **a**). The mechanism deflection rotates the curved lever (circle 1), i.e., the circular arc profile in **b**). The red line in **c**) is perpendicular to the deflected circular arc (circle 2) and goes through the center of the circular arc. Using its inclination (δ), the pressure angle (α) can be calculated.

The actuator state is determined based on angles φ_s and φ_d , which represent the stiffness motor rotation that corresponds to the follower rotation, and the angular deflection of the mechanism, respectively. Geometrically, the mechanism represents the interaction between a line (line 1 in Fig. 3(a)) and a circle (circle 1 in Fig. 3(a)) governed through equations:

$$y = \tan\left(-\frac{\pi}{2} + \varphi_{\rm s}\right) x + (R_{\rm s} + R_{\rm b}), \tag{1}$$

$$R_{\rm s}^2 = (y - (R_{\rm s} + R_{\rm b}))^2 + x^2.$$
 (2)

To calculate all the torques, the first step is to calculate the intersection point between the line (line 1) and the circle (circle 1), with coordinates (x,y) (see the red dot in Fig. 3) using equations (**a** is introduced to shorten them):

$$x(\varphi_{d}, \varphi_{s}, R_{s}, R_{b}) = (R_{b} + R_{s})\sin(\varphi_{s})\left(2\sin\left(\frac{\varphi_{d}}{2}\right)\sin\left(\frac{\varphi_{d}}{2} - \varphi_{s}\right) + \mathbf{a}\right), \quad (3)$$

$$y(\varphi_{d}, \varphi_{s}, R_{s}, R_{b}) = (R_{b} + R_{s})\cos(\varphi_{s}) \left(\cos(\varphi_{d} - \varphi_{s}) + \frac{\sin^{2}(\varphi_{s})}{\cos(\varphi_{s})} - \mathbf{a}\right), \quad (4)$$

$$\mathbf{a} = \sqrt{\frac{R_{\rm s}^2}{(R_{\rm s} + R_{\rm b})^2} - (\sin(\varphi_{\rm d} - \varphi_{\rm s}) + \sin(\varphi_{\rm s}))^2}.$$
 (5)

The spring is the force generating element, and it lies on the line with an inclination based on the cam follower angle, φ_s . The force (F_{spr}) is calculated via the compression (d) obtained through the distance (D) (see Fig. 3(b)):

$$D = \sqrt{(x - x_{\rm c})^2 + (y - y_{\rm c})^2},$$
 (6)

$$d = R_{\rm S} - D,\tag{7}$$

$$F_{\rm spr} = k_{\rm int} d. \tag{8}$$

The known line 1 and the deflected circle 2 (φ_d) geometry can be used to calculate the pressure angle(α)(note that $x_c = 0, y_c = R_s + R_b$) using equations:

$$x_{\rm nc} = x_{\rm c}\cos(\varphi_{\rm d}) - y_{\rm c}\sin(\varphi_{\rm d}),\tag{9}$$

$$y_{\rm nc} = y_{\rm c}\cos(\varphi_{\rm d}) + x_{\rm c}\sin(\varphi_{\rm d}), \tag{10}$$

$$\delta = \arctan\left(\frac{y - y_{\rm nc}}{x - x_{\rm nc}}\right) + \frac{\pi}{2},\tag{11}$$

$$\alpha = \delta - \varphi_{\rm s}. \tag{12}$$

Here the new circle center coordinates (x_{nc}, y_{nc}) are calculated through the rotation/deflection (ϕ_d) of the original circle center (x_c, y_c) . The δ is the inclination of a line going through (x, y) and (x_{nc}, y_{nc}) , which is perpendicular to the lever, i.e., it goes through the rotated circle center, and is therefore required to calculate the pressure angle (α) . The $\pi/2$ in (11) represents the complementary angle. The deflection torque (τ_d) is found using vector cross product:

$$F = F_{\rm spr}/\cos(\alpha),\tag{13}$$

$$\vec{F} = F\left[\cos\left(-\pi/2 + \varphi_{\rm s} + \alpha\right), \sin\left(-\pi/2 + \varphi_{\rm s} + \alpha\right), 0\right],\tag{14}$$

$$\vec{r} = [x, y, 0] \tag{15}$$

$$\vec{\tau}_{\rm d} = \vec{r} \times \vec{F} \,. \tag{16}$$

The deflection torque derivative can be used to find the theoretical stiffness of the mechanism stiffness (K):

$$K = \frac{d\tau_{\rm d}}{d\varphi_{\rm d}}. (17)$$

At any given state (φ_s, φ_d) , the torque (τ_s) required to hold a desired stiffness, angle φ_s , is calculated as

$$F_{\rm din} = F_{\rm spr} \tan(\alpha), \tag{18}$$

$$\tau_{\rm s} = F_{\rm din} D. \tag{19}$$

 $F_{\rm din}$ is the tangential force which appears due to the rising pressure angle and because the system is not completely perpendicular to the load. Lastly, if information about the amount of the stored elastic energy ($E_{\rm sys}$) is desired, the following equation can be used to attain it:

$$E_{\rm sys} = \int_0^{\varphi_{\rm d}} \tau_{\rm d} d\varphi_{\rm d}. \tag{20}$$

3.3. Theoretical results

To analyze the mathematical model, the parameters collected in Table 1 are used to calculate it and to build a prototype.

Parameter	Value	Unit	Parameter	Value	Unit
$R_{\rm s}$	50	[mm]	$R_{\rm b}$	0	[mm]
$k_{ m int}$	72.6	[N/mm]	$k_{ m lin}$	0-49	[Nm/rad]
$oldsymbol{arphi}_{ ext{S}}$	0-80	[°]	$arphi_{ m d}$	± 20	[⁰]
$ au_{ m p,nom}$	15	[Nm]	$ au_{ m s,nom}$	5	[Nm]
$ au_{ m p,peak}$	22.5	[Nm]	$ au_{ m s,peak}$	6.3	[Nm]
$t_{ m S}$	0.15	[s]			

Table 1: Mathematical model parameters

The base geometry is defined by the stiffness radius R_s . The R_b value is purely design based and introduces the flexibility for an easier bearing placement at axis A. In the proposed prototype, the bearing of the circular-arc lever was moved behind the plane of the follower mechanism, consequently the R_b is equal to zero. The increase of the R_b value introduces the possibility of a flatter future design, where the bearing is placed in plane of the follower mechanism.

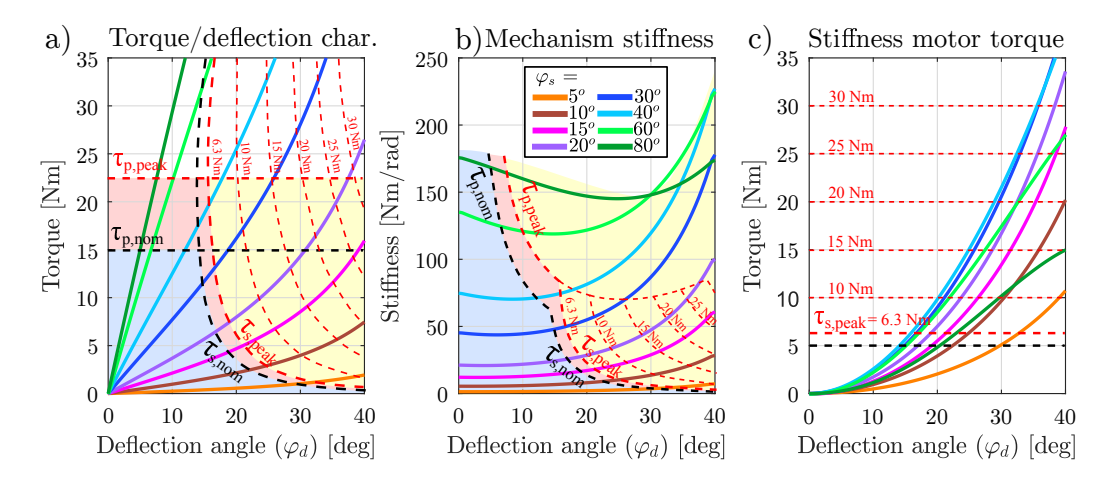


Figure 4: The torque required to deflect the mechanism is shown in **a**). Its derivation or stiffness is shown in **b**). The torque required to hold a given stiffness resulting from the tangential force is shown in **c**). The line colors represent a specific stiffness setup angle. The **black and red dashed lines** represent the nominal and peak torque for both motors. Additional **red dashed lines** represent the torque limits for stronger stiffness motors. The **blue**, **red and yellow areas** represent the below nominal, below peak and above actuator peak torque operation regions. Assuming the position motor can be backdriven in loads above its current limit (gearbox peak torque), the **white areas** in **a**) and **b**) cannot be reached in theory.

The torque limits of both motors resulting from their gearboxes are marked in Table 1. The nominal and peak torques of the position motor are marked as position motors ($\tau_{p,nom}$, $\tau_{p,peak}$), and for the stiffness motor as ($\tau_{s,nom}$, $\tau_{s,peak}$). The reader should note that the theoretical results assume and evaluate the case where a position motor is placed directly at Pivot A. In the prototype implementation, however, the motor is connected to the pivot A through a bidirectional cable system. Fig. 4 shows the theoretical torque/deflection and stiffness/deflection characteristics, calculated using values from Table 1 for different cam follower angles.

The size of the torque/deflection space of the mechanism is determined through the motor and gearbox torque limits. In Fig. 4, they are marked with the red and black dashed lines in all graphs. Through them, the torque/deflection space is split into four regions using the proposed model and numerical calculations. Areas colored in blue and red (see Fig. 4(a)) represent actuator operation below nominal and peak torques, respectively, for both motors used. The yellow area marks the region where the torque required to hold the stiffness is higher than the stiffness motor gearbox limit. Here, the stiffness motor cannot adjust the stiffness anymore and due to a high gearbox transmission, the gearbox can get damaged. The spe-

cific ways to account for this are discussed in Section 6. Additional red dashed lines are drawn to show how a potentially stronger stiffness motor affects and increases the peak operation area. Similarly, if the external torque is above the limit of the position motor (or its gearbox), it cannot move or is back-driven, depending on the gearbox transmission type and the set current limit. Since the motor can be back-driven in case of an overload, the white region in Fig. 4(a,b) is theoretically unreachable.

Looking at the characteristics, one can observe two advantages. The first is the nearly-linear (pseudo-linear) torque/deflection characteristics, which is the strongest in the operational area of the motor (see Fig. 4(a,b)). The pseudo-linear expression is used to denote that although the mechanism is in principle nonlinear, it can be approximated as linear in the working space with a good precision. Through the use of linear regression in the area below the peak motor conditions, this feature is exploited to reduce the model dimensions. While linear regression can be performed also above peak motor conditions, since the actuator does not operate in that region, regression precision is improved by staying below the peak conditions. The possibility to use a linearized model eases the mechanism design and allows application of simpler control algorithms. See the linear regression results in Fig. 5(a,b).

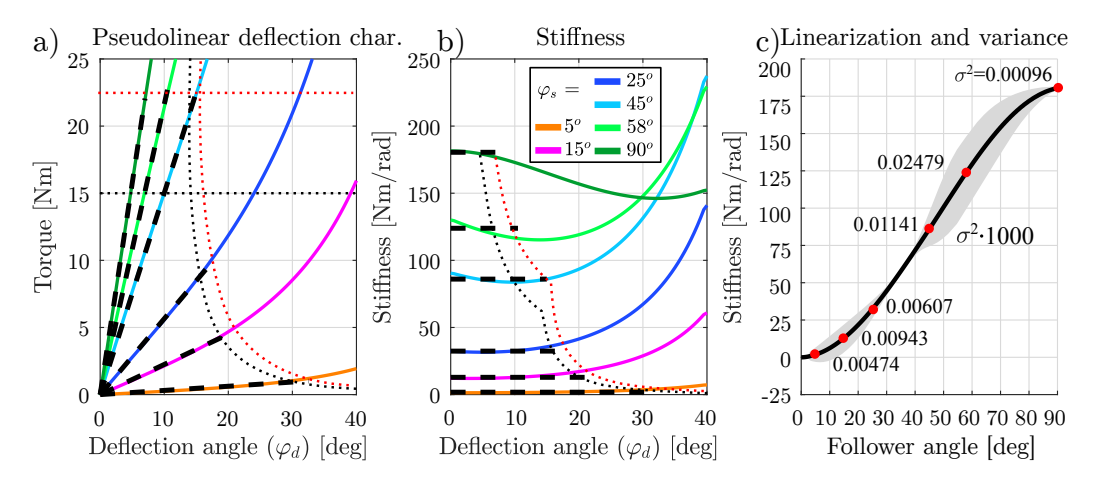


Figure 5: The external torque required to deflect the mechanism is shown in **a**) for different cam follower angles. Its derivative, i.e., mechanism stiffness, is shown in **b**). The **black** and **red dotted lines** show the torque limits of both motors. The **black dashed lines** in **a**) and **b**) show the results of the linear regression. Based on the regression result, a relation between the cam follower angle and the resulting mechanism stiffness approximation can be constructed, shown in **c**). The **gray area** represents the linear regression error variance (scaled 1000x).

The regression is performed with the assumption that all the lines start at the origin. As seen in Fig. 5(c), a relation between the cam follower angle and the actual mechanism stiffness is thus created. In this specific case, a look-up table can be built to represent that relation to transform the cam follower angle to the actual stiffness and vice-versa. Observe that the linear regression of the theoretical model introduces only small errors, emphasized in Fig. 5(c), which shows the linear regression error variance. The data had to be up-scaled 1000 times to appear on the plot.

The second mechanism advantage is the low stiffness variation torque (see Fig. 4(c)), which is far lower than the values for the position motor (see Fig. 4(a)). Thus, compared to the position motor, a less powerful motor can be used to vary the stiffness. Of course, it also depends on the desired speed of stiffness variation. However, observe that while initially the torque to hold the stiffness is small, with the increase of the deflection angle, the torque rapidly increases (see Fig. 4(c)).

4. Experimental prototype and control

A prototype was built not only to validate the proposed stiffness validation approach, but to later serve as an actuator of a wearable device. This is why experiments are made by exploiting the sensor redundancy and the fact that the actuator is a fully functional device and can provide monitoring data. Table 2 collects standard components that make up the VSA.

Table 2: Actuator components

Component	Description	Further data		
Position motor	DCX35L GB KL 48V	Maxon 80W, 113:1		
Stiffness motor	DCX22L GB KL 48V	Maxon 20W, 172:1		
Motor amplifier	ESCON 50/5	one for each motor		
Incremental encoders	4 encoders RLS	RM22, RoLin		
Torque sensor	Tovey Engineering	RT-500, 55Nm		
Controller	PCM-3362 PC-104	integrated circuit		
Data acquisition	Sensoray 526			

To provide sufficient actuation, Maxon motors are used due to their high power-to-weight ratio; an 80W version for the position setup and a 20W version for the stiffness variation. Both motors use planetary gear transmissions, at ratio 113:1 for the position setup and 172:1 for the stiffness setup. Note that the

nominal and peak torques presented in Table 1 stand for the respective planetary gear transmissions, and not the motors themselves. The position motor gearbox has a 72% efficiency and a 1° backlash, while the stiffness-motor gearbox has a 75% efficiency and a 1.1° backlash. Each motor has its own dedicated Maxon ESCON 50/5 amplifier, which provides current feedback and the option to control the motor either in velocity or current input mode.

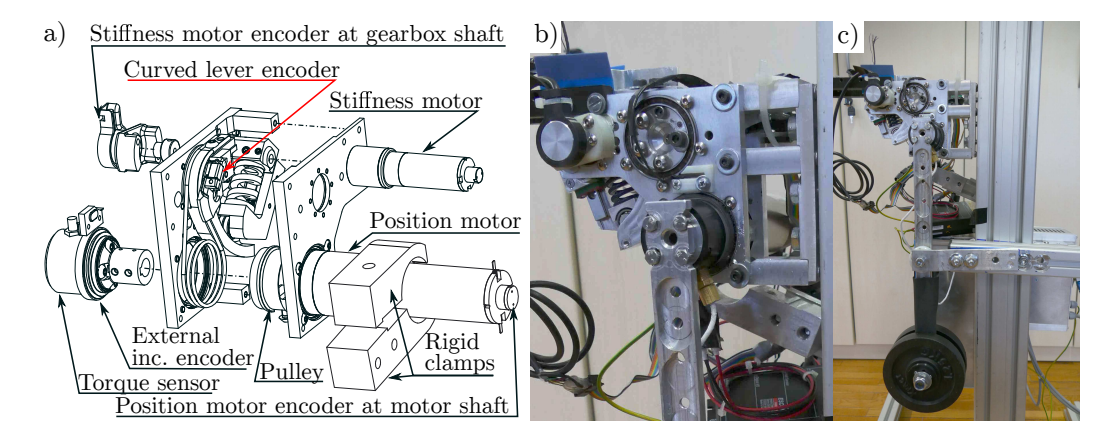


Figure 6: An exploded CAD model view of the experimental actuator is depicted in **a**). The actual implementation is shown in **b**). The experimental system, where the external link is fixed to enable the measurement of the internal actuator characteristics, is represented in **c**).

Fig. 6(a) shows the location of the mechanical components. The prototype system is fully sensorized with 4 incremental encoders, one before the position motor gearbox, one after the stiffness motor gearbox, one at the circular arc lever and one at the external link. This provides a sensor redundancy. A compact reaction torque sensor RT-500, rated to 55Nm, provides additional information about the external torque for validation purposes. Note that a compact commercial unit could be constructed with fewer sensors. The main controller is composed of a PCM-3362 PC-104 integrated circuit with a Sensoray 526 data acquisition card. The Sensoray 526 allows 4 programmable counters to directly count incremental encoders and 8 A/D converters. Additional sensors can be added to the system aimed at human-robot collaboration, like EMG (electromyography) electrodes. The system is compatible with Simulink Real-TimeTM software and provides real-time control at 1000Hz and synchronised data acquisition.

In this work, two experiments were performed to evaluate the device. One is intended to measure the torque/deflection characteristics. The other is intended to measure the stiffness variation speed. The control for the position motor differs

between the experiments. The control of the stiffness motor, however, stayed the same. All control algorithms are gathered in Table 3.

Table 3: Control algorithms

Experiment	Motor/mod	le Control algorithm	
Characteristic		$u_{\text{pos}} = K_{\text{p,ff}}\dot{\theta}_{\text{p,des}} + PD(\theta_{\text{p,des}} - \theta_{\text{p,m}})$	(21)
measurement	/position	pos pin piacs (piacs pinn)	` /
Stiff. varia-	P. motor	J	
tion speed	/torque	$u_{\text{pos}} = \tau_{\text{des}} K_{\text{ff}} + \ddot{\tau}_{\text{des}} \frac{J}{K_{\text{c}}} + PD(\tau_{\text{des}} - \tau_{\text{ext}}) + \dot{\theta}_{\text{p,m}} K_{\text{f}} +$	$-\theta_{\rm ext}JK_{\rm b}$
	•	5	(22)
All	S. motor	$u_{\text{stiff}} = K_{\text{s.ff}} \dot{\theta}_{\text{s.des}} + PD(\theta_{\text{s.des}} - \theta_{\text{s.m}})$	(23)
	/position	$u_{\text{Stiff}} - H_{\text{S,ff}} \sigma_{\text{S,des}} + HD(\sigma_{\text{S,des}} - \sigma_{\text{S,m}})$	(23)

P. motor is the position motor and S. motor is the stiffness motor.

To control the position motor during the torque/deflection characteristics measurements, a position feedback controller with feed-forward terms (21) was used, using velocity as an input. Here, the $K_{\rm p,ff}$ is the feed-forward term. For the stiffness variation speed experiment, a torque controller adopted from [11] and [36] was used with motor current as the input into the motor controller. Due to the pseudo-linear behavior of torque curves, one can apply the same controller. Additionally, the external link acceleration is used as feedback to account for spring oscillations with an added friction compensation term. In this case, $K_{\rm ff}$ is the feedforward term, J and $K_{\rm s}$ represent the inertia and stiffness of the elastic element, $K_{\rm f}$ is the friction compensation term and $K_{\rm b}$ is the acceleration feedback term. During the experiment, it was commanded to hold a specific torque while a fast stiffness variation command was issued to the stiffness motor.

To control the stiffness motor position during both experiments, a simple position feedback controller with feed-forward terms was implemented (23) using velocity as the input into the motor controller. Here, $K_{s,ff}$ is the feed-forward term of the stiffness motor. More about the specific experiments is written in their respective result sections.

The testing experimental configurations are shown in Fig. 6(b,c). At present, all the equipment is mounted on an aluminum column, which facilitates a faster development cycle. However, all components were chosen or designed with a potential future wearable application in mind and are as small as feasible.

5. Experiments and results

5.1. Torques of the internal mechanism

The sensorized system was exploited to directly measure the torque/deflection characteristics of the internal mechanism, and the required torque to hold a given stiffness. For this particular measurement, the external link was fixed (see Fig. 6(c)), and the position motor performed movements using position control. Since the external link is fixed, a position motor movement directly compresses the internal mechanism and thus enables a straightforward way to rotate the deflection lever to a desired location. The position motor was commanded to slowly move in one direction until either the position motor current limit (1.9A or approx. 15Nm), or the current limit of the stiffness motor (0.55A or approx. 4.3Nm), or the curved link deflection limit (predetermined angle $\varphi_d = 17^o$) was reached. The gathered torque sensor data can now be compared to the movement of the curved lever to arrive at the internal mechanism characteristics. Fig. 7(a) shows the results.

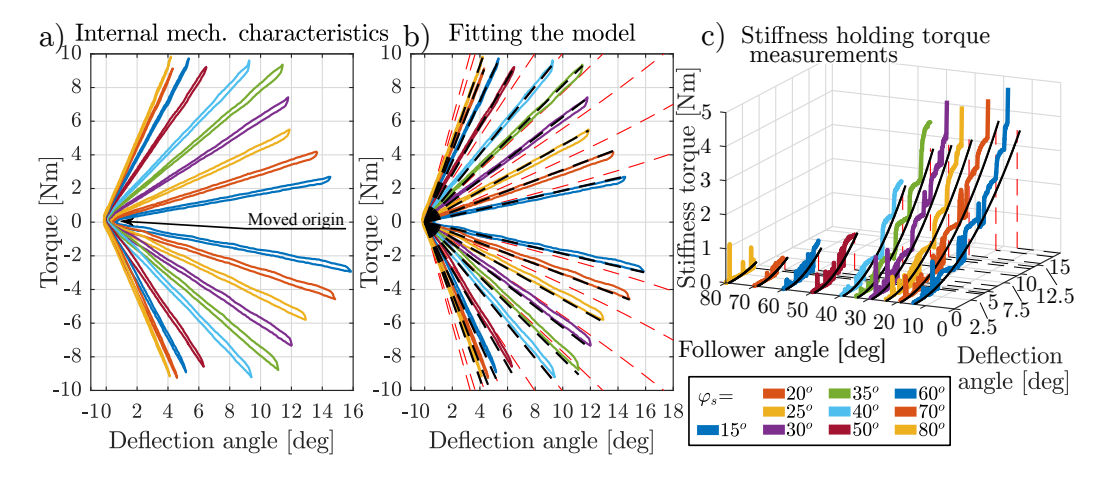


Figure 7: The measured relation between the torque and the deflection of the curved lever shown in **a**) represents the internal mechanism characteristics for different cam follower angles. In b), the theoretical model **red dashed** and a linear regression of the measurements **black dashed** are added to the initial measurements. The torque required to hold a given stiffness, calculated based on the motor current measurement, is in **c**) compared to its theoretical model (**black line**).

Observe also the moved origin phenomena in Fig. 7(a). It is a consequence of the light preload preventing the cam follower from lifting up and loosing contact with the cam curve, since there is no load on the cam spring follower at zero deflection. This, in combination with the tension mechanism, reduces the nonlinearities effect of the steel cables in the external mechanism. But, as a consequence,

the torque/deflection curves slightly miss the origin of the torque/deflection space in the internal mechanism. The slight preload should not be confused with the preloadless stiffness variation [15, 26].

The data contains some discrepancy between the measurements and the plain mathematical model (see the red dashed lines in Fig. 7(b)). This is attributed to all the system nonlinearities that are also hard to model and further elaborated in the discussion. To find the real linear characteristics of the internal mechanism, a linear regression is performed over the loading phases of both directions. The linear regression results are shown in Fig. 7(b) in black dashed lines. The regression effectively provides the relation between the desired internal mechanism stiffness and the required cam follower angle to achieve it.

The next important thing is the torque (of the stiffness motor) required to hold the desired stiffness (see Fig. 7(c)). The mathematical model nicely follows the stiffness motor torque at different deflection angles. In this measurement, again, the experimental system is exploited and the motor current is used to approximate its torque. This, and the fact that the motor is position controlled, can be attributed to different discrepancies of the real-system measurement. Such effects, including the bearings or gearbox nonlinearities, are not modeled and accounted for at this stage.

5.2. Bidirectional transmission or external mechanism

The main part of the external mechanism is the cable transmission that allows for a bidirectional application of the proposed VSA. To determine its characteristics, the torque sensor measurements are used in combination with position motor movement. See Fig. 8(a) for the results. These measurements are influenced by the position motor gearbox backlash, the tension, elastic deformation and bending of the steel cable and the bearing friction. As seen in 8(a), these effects culminate in deflection torque, which – compared to the internal mechanism – appears much less linear. One can also observe that, again, the lines are not exactly symmetrical or centered, specifically at zero-crossing. This, however, depends on the calibration of the system. While the use of a cable transmission is generally rather simple, overall, the use of the steel cable increased the non-linearity of the system and its hysteresis. Such nonlinearities of cable transmission are common, and also present in other types of VSAs that use similar technology [37].

A linear regression was performed to construct an approximated linear stiffness model of the external mechanism. It is shown in Fig. 8(b) in black dashed lines and the mathematical model in red dashed lines. The linear approximation still nicely follows the measured data. The results gathered were also used to

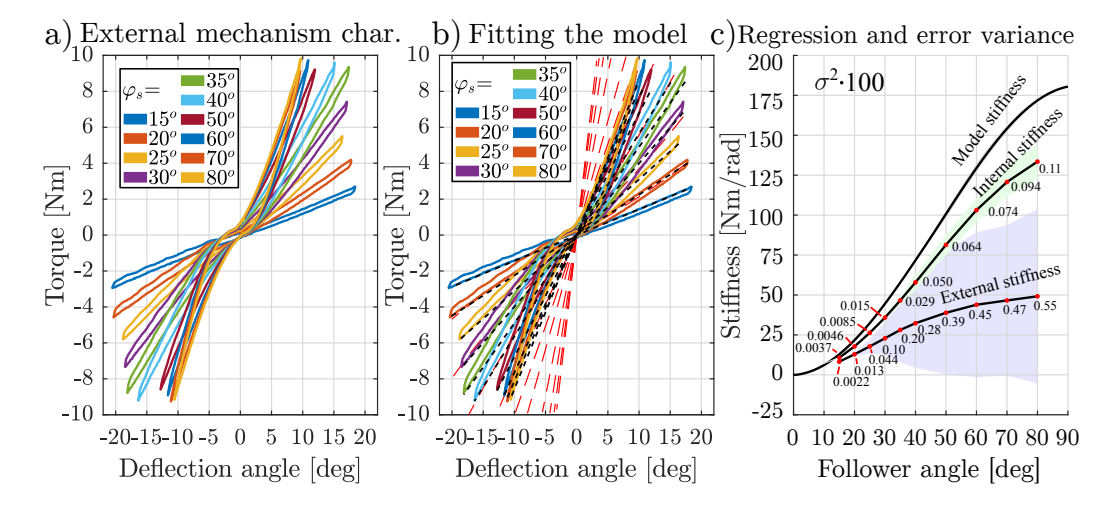


Figure 8: The torque required to deflect the VSA, i.e., the external mechanism, is presented in **a**). In **b**), the theoretical model (**red dashed lines**) and the linear regression lines (**black dashed lines**) are added to the measurements. The approximated resulting stiffness in relation to the cam follower angle is represented in **c**) for different stages of the mechanism. These include the ideal theoretical relation, the internal mechanism and the external mechanism. The colored areas represent the linear regression error variance (scaled 100x).

construct a look-up table to be used in control and to transform the cam follower angle to the desired mechanism stiffness for the experiment in Section 5.3.

The error-variances of the linear-regressions are shown in Fig. 8(c) and enable the comparison of linearity error between different stages of the mechanism. The mathematical model stiffness, internal mechanism and the external mechanism stiffness are all marked on the graph. One can observe that the cable mechanism reduced the maximal stiffness of the internal device from 0-130 Nm/rad to 0-49 Nm/rad, as measured on the external mechanism. Similarly, one can observe in the error variance that the linearity is lower in the external mechanism as compared to the internal mechanism. In the external mechanism, the regression error increases with higher stiffness or at higher loads.

5.3. Stiffness variation speed

An important feature is the easy stiffness variation enabled by the preloadless mechanical principle. In the prototype, this feature is exploited for a quick stiffness variation. However, one could also exploit it to use a smaller and lighter stiffness motor and therefore reduce the overall device weight.

For this experiment, a specific torque was commanded to the position motor using the torque controller described in Table 3. Since the external link is fixed,

the position motor torque directly loads the spring and thus simulates an external load. After that, a step input is commanded to the stiffness setup motor to achieve a stiffness change from 27Nm/rad to approximately 46Nm/rad. The results are shown in Fig. 9(a) for different external loads. The cam follower angle used

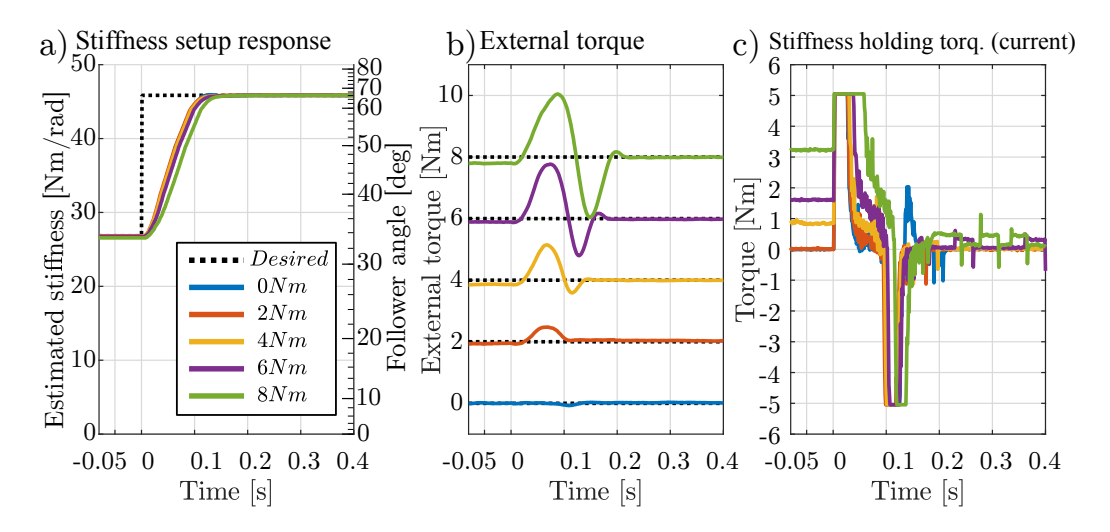


Figure 9: The stiffness motor is commanded to perform a stiffness jump from 27 to 46 Nm/rad in a) under different external loads. The equivalent follower angle is depicted on the right axis. In b), the corresponding external torque is shown. The torque required to perform the jump on the velocity-based position controlled motor is shown in c). The motors electric current is used to approximate its torque.

in previous graphical representations is here transformed to its linear mechanism stiffness approximate using the above mentioned linear regression results, i.e., the look-up table. The estimated stiffness is thus shown on the left axis. The corresponding follower angle is shown on the right axis. The stiffness change was equally fast for all the cases, just below 0.15s. The external torque during a corresponding measurement is shown in Fig. 9(b). The fast follower rotation, i.e., the cam follower angle variation, can cause a disturbance on the external torque due to inertia, mechanism pressure angle and spring potential energy. However, the position motor torque controller is able to diminish this disturbance, as seen in Fig. 9(b).

In Fig. 9(c), the measured actuation current of the stiffness motor is shown.

The current of the stiffness motor is limited for hardware safety reasons. 1 The limit is estimated to \sim 5 Nm on the axis of the planetary gearbox, which is the specified nominal gearbox limit (see also Table 1).

6. Discussion

6.1. Comparison to other VSAs

In this Section the properties of the proposed actuator are evaluated in light of the MACCEPA, the FS-Joint and the AwAS. These actuators were chosen due to their frequent use in the literature. Their performance properties were collected from the literature and gathered in Table 4, their components in Table 5 and their geometric properties in Table 6. The reader should note that exact comparisons are difficult if not impossible due to a lack of available information and actuator operation principles. Note also that these actuators should be treated as research prototypes and are likely over-dimensioned, have redundant components and that each might target a specific application. For an exact comparison, one would have to construct all these mechanisms using the same motors and springs, and then compare them.

In Table 4, one can observe that the FS-Joint implements a very rigid spring. And that the MACCEPA actuator has the largest deflection range and the ability to

Actuator	Max.	Spring	Actuator	Max.	Defl.	Stiffness
	torque	used	stiffness	elastic	range	variation
	[Nm]	[N/mm]	[Nm/rad]	energy [J]	[°]	time [<i>s</i>]
MACCEPA [27, 38]	70	64.8	5-110	27.9	±60	2.6
FS-Joint [14, 28]	67	908	826	5.3	± 15	0.33
AwAS [15]	80	80	30-1300	3.5	± 14	4-6
PLVL-VSA	22.5	72.6	0*-49	3	± 20	0.13

Table 4: Actuator comparison - part I - performance

store the largest amount of elastic energy. In Table 5, observe that the MACCEPA implements a more powerful stiffness motor, but still achieves a relatively slow

^{*}Zero stiffness results in almost unobstructed external link movement inside the deflection range $\pm 20^{\circ}$. It can be exploited for sensor calibration.

¹The torque approximation is not precise and does not take into account the properties of the gearbox. A complex system to exactly approximate the torque would only slightly change the torque limit.

Table 5: Actuator comparison - part II - components

Actuator	Position motor	Gearbox	Stiffness motor	Gearbox
	(power)		(power)	
MACCEPA	Powermax 30	(74x3.8):1	Powermax 20	(19x24):1
[27, 38]	Maxon (200W)	GP42C	Maxon (120W)	GP22HP
FS-Joint	Robodrive ILM	80:1 HD	Robodrive ILM	1000:1? ¹
[14, 28]	50x14 SP (180W)	CSD-25	25x8 SP (60W)	
AwAS-I	Emoteq, Inc.,	50:1	Faulhaber,	$(23x?^1):1$
[15]	HT-02300 (56W)	HD^2	EN-1727C (2.5W)	Series 17/10
PLVL-VSA	Maxon DCX35L	113:1	Maxon DCX22L	172:1
	(80W)	GPX42 C	(20W)	GPX26 C

¹unknown/unspecified additional component

stiffness variation (2.6s from 3% to 97% [38]). This is the direct consequence of the parallel stiffness variation mechanism. Observe also that the AwAS actuators stiffness motor is the least powerful. Consequently, its stiffness variation is rather slow (4 - 6 s) but comparable to that of the MACCEPA. Using a perpendicular way of stiffness variation, like in AwAS, enables a more efficient stiffness variation. Observe that the proposed prototype uses a low power motor and allows a very fast stiffness adaptation. However, this feature can also be exploited in favor of lower stiffness motor torque, and thus a weaker motor.

In the last Table 6 the bare mechanism mass is introduced to reduce the vari-

Table 6: Actuator comparison - part III - geometry

Actuator	Mechanism	Volume	Full	Position	Stiffness	Mechanism
	dim. [cm]	$[cm^3]$	mass	motor	motor	mass ⁴
			[kg]	[kg]	[kg]	[kg]
MACCEPA [27, 38]	/	/	2.4	0.63	$0.18+?^{1}$	1.6
FS-Joint [14, 28]	Ø9.5 x 12	851	1.4	0.39	0.25^{3}	0.77
AwAS-I [15]	31 x 14 x 7	3038	1.8	0.79	$0.07+?^{1}$	0.95
PLVL-VSA	12 x 11 x 4	528	1.9	0.85	0.20	0.85

¹unknown/unspecified additional component

ability of mass data. It is calculated through the deduction of the combined motor mass from the overall mass of the mechanism. However, the mass data is espe-

²unknown component, Harmonic Drive CSD-25-50-2A-GR is used

³unknown mass, Maxon motor planetary gearbox (GP32C) is used

⁴Mechanism mass = Full mass - Position motor - Stiffness motor

cially hard to compare, so no explicit conclusions can be derived in this regard. Observe that while the AwAS has advantages, one can see that its mechanism volume is quite high (see Table 6). A lot of space is used up by the linear bearings rails that also need to be sturdy enough to minimally deflect under load, and by the symmetrical spring arrangement, which also increases the actuators overall size. The PLVL-VSA perhaps most closely resembles the AwAS actuator. Contrary to the AwAS, it allows for a rotational based stiffness variation. This allows the replacement of the long linear guides with rotational bearings, and thus severely reduces the overall size of the actuator.

The reader can see that a linear bearing is also used in the proposed PLVL-VSA design (see Fig. 1), but its role is different than in the AwAS, since it does not need to bear the full spring load. It is intended to prevent the spring from buckling and to bear the tangential force that appears due to the pressure angle. Additionally, only one compression spring is used, which further reduces the size and number of parts. As seen in Table 6, this results in a more compact actuator.

A cable transmission is then used to enable a bidirectional application and make the VSA-actuator fully functional. The actuator keeps most of the AwAS actuator advantages, such as pseudo-linear torque/deflection characteristics and the variable-ratio lever stiffness variation principle. At higher deflection a tangential force resisting the stiffness motor motion appears, because the stiffness variation is not completely perpendicular anymore. The same force appears also by AwAS actuator [15]. This can either be avoided by staying below a certain deflection, like in AwAS, or by staying above a certain level of stiffness or by using a stronger stiffness motor.

6.2. Discussion

Overall, the proposed Pseudo-linear Variable-Lever Variable-Stiffness Actuator shows promising results, and a distinction to other relevant VSAs, namely the MACCEPA [39], the DLR FSJ [14] and the AwAS [15]. The presented results show that the internal mechanism behaves as the model predicted. The full VSA includes the cable transmission, and its non-linearities pose some difficulties, if one desires accurate torque control combined with very accurate position control. However, this is a common feature of cable transmissions, bypassed through accurate models and frequent calibration [40]. For the proposed mechanism, the cable transmission is suitable for lower torques and lower stiffness settings. Fig. 8(b,c) show that lower stiffness settings retain the (desired) linearity. In higher stiffness settings and higher torque loads, the nonlinearities and hysteresis increase.

The cable transmission requires proper cable tension and minimal stretching of the cable. The latter can be accomplished by choosing a strong cable, which is thick and has a rigid strand configuration. However, since the pulley of the transmission is relatively small, choosing a thick, strong cable, increases its bending torque effect and consequently drastically increases the introduced nonlinearities. A 1.8 mm diameter stainless steel cable with a 7x7 strand geometry was used in the end. Some difficulties of the proposed case could be reduced by implementing pulleys of larger diameter, if the application allows it. A contributing factor is also the friction in bearings. To reduce this effect, unsealed bearings were chosen with a larger safety factor or even double-row types. This reduced the internal forces and therefore friction.

One difficulty which still persists in the design of the proposed mechanism is the rising pressure angle. For research purposes, the problems can be avoided by staying in stiffness settings above 15 Nm/rad. To reduce the device complexity, this was the option chosen during the experiments. However, to fully utilize the advantages of preloadless design, the first option is to sacrifice some stiffness variation speed and use a higher transmission ratio in the stiffness motor. Consequently, the torque/deflection area of the proposed mechanism, as marked in Fig. 4 would also increase. This can be achieved by implementing a worm gear transmission which would also make the stiffness setup mechanism non-backdrivable, meaning that no energy would be needed to hold a given stiffness. Another way to keep the same motor and still achieve an increase of torque/deflection space is to exploit the external torque. One can use it to help the stiffness motor by an addition of a second spring connected between the curved lever and stiffness motor. This is theoretically explored in [41].

In the experimental evaluation, the torque sensor plays an important part. The actuator, however, is intended to function without it, since its removal can severely decrease the cost of such a device. The presented implementation does have some drawbacks in that regard. The first stems from the cable non-linearities, which make the measurement of the compression at the external link not reliable at low torques. The second difficulty lies in the inability to infer the direction of the external load based on the elastic element compression measurement. The compression direction can be derived using other encoders. But, since the external link encoder also measures the backlash in the position motor gearbox, smaller loads tend to oscillate around zero. This is why in the current case, the torque sensor is also used to determine the external load. However, with a more strategic placement of the position encoder sensor, a measurement devoid of position motor backlash could be achieved in future iterations.

While the proposed variable stiffness mechanism has many benefits despite some nonlinearities, in the future, effort will be made to replace the cable transmission with a more rigid solution. Thus, the properties of the internal mechanism will be directly transferred to the external system.

7. Conclusion and further work

The fully sensorized actuator was designed to serve as the means for high level exoskeleton control algorithms studies. The characteristics of the proposed mechanism were chosen to facilitate such studies. The novel variable stiffness mechanism results in a pseudo-linear torque-deflection characteristics with a rotational stiffness variation. The last enables a more compact mechanism design. A more convential control and easier mechanism dimensioning is enabled by the mechanism's pseudo-linearity.

An advantage is the preloadless design, where either a fast stiffness variation, or a low-torque one can be achieved. The ability to use a lower power stiffness motor is convenient when following the recent trend of actuator weight reduction, and compact design. The proposed mathematical model was verified, showing great coherence with the internal mechanism behavior. It can serve to either find a suitable combination of components, or to find further solutions.

While there are drawbacks of the proposed overall actuator implementation, originating in the cable transmission, the results are encouraging and not detrimental for future exoskeleton applications. Future studies will explore the effect of the actuator properties for wearable applications.

8. References

- [1] L. M. Mooney, E. J. Rouse, H. M. Herr, Autonomous exoskeleton reduces metabolic cost of human walking during load carriage, Journal of Neuroengineering and Rehabilitation 11 (2014) 80–91. doi:10.1186/1743-0003-11-80.
- [2] J. Zhang, P. Fiers, K. A. Witte, R. W. Jackson, K. L. Poggensee, C. G. Atkeson, S. H. Collins, Human-in-the-loop optimization of exoskeleton assistance during walking, Science 356 (2017) 1280–1284. doi:10.1126/science.aa15054.

- [3] M. Kim, Y. Ding, P. Malcolm, J. Speeckaert, C. J. Siviy, C. J. Walsh, S. Kuindersma, Human-in-the-loop bayesian optimization of wearable device parameters, PLOS ONE 12 (2017) e0184054. doi:10.1371/journal.pone.0184054.
- [4] N. G. Tsagarakis, D. G. Caldwell, F. Negrello, W. Choi, L. Baccelliere, V. G. Loc, J. Noorden, L. Muratore, A. Margan, A. Cardellino, et al., WALK-MAN: A high-performance humanoid platform for realistic environments, Journal of Field Robotics 34 (2017) 1225–1259. doi:10.1002/rob. 21702.
- [5] L. Colasanto, N. G. Tsagarakis, D. G. Caldwell, A compact model for the compliant humanoid robot COMAN, Proceedings of the 4th IEEE RAS & EMBS International Conference on Biomedical Robotics and Biomechatronics (BioRob), 1 (2012) 688–694. doi:10.1109/BioRob.2012.6290765.
- [6] A. Parmiggiani, G. Metta, N. Tsagarakis, The mechatronic design of the new legs of the iCub robot, Proceedings of the 12th IEEE-RAS International Conference on Humanoid Robots (Humanoids) 1 (2012) 481–486. doi: 10.1109/HUMANOIDS.2012.6651563.
- [7] D. W. Haldane, M. M. Plecnik, J. K. Yim, R. S. Fearing, Robotic vertical jumping agility via series-elastic power modulation, Science Robotics 1 (2016) eaag2048. doi:10.1126/scirobotics.aag2048.
- [8] B. Kim, A. D. Deshpande, Design of nonlinear rotational stiffness using a noncircular pulley-spring mechanism, ASME Journal of Mechanisms and Robotics 6 (2014) 041009. doi:10.1115/1.4027513.
- [9] N. Vitiello, T. Lenzi, S. Roccella, S. M. M. De Rossi, E. Cattin, F. Giovacchini, F. Vecchi, M. C. Carrozza, NEUROExos: A powered elbow exoskeleton for physical rehabilitation, IEEE Transactions on Robotics 29 (2013) 220–235. doi:10.1109/TRO.2012.2211492.
- [10] D. Maeda, K. Tominaga, T. Oku, H. T. Pham, S. Saeki, M. Uemura, H. Hirai, F. Miyazaki, Muscle synergy analysis of human adaptation to a variable-stiffness exoskeleton: Human walk with a knee exoskeleton with pneumatic artificial muscles, Proceedings of the 12th IEEE-RAS International Conference on Humanoid Robots (Humanoids) 1 (2012) 638–644. doi:10.1109/HUMANOIDS.2012.6651587.

- [11] G. A. Pratt, M. M. Williamson, Series elastic actuators, Proceedings of the IEEE/RSJ International Conference on Intelligent Robots and Systems 1 (1995) 399–406. doi:10.1109/IROS.1995.525827.
- [12] M. Grimmer, M. Eslamy, S. Gliech, A. Seyfarth, A comparison of paralleland series elastic elements in an actuator for mimicking human ankle joint in walking and running, Proceedings of the IEEE International Conference on Robotics and Automation (ICRA) 1 (2012) 2463–2470. doi:10.1109/ ICRA.2012.6224967.
- [13] S. Arumugom, S. Muthuraman, V. Ponselvan, Modeling and application of series elastic actuators for force control multi legged robots, J. of Computing 1 (2009) 26–33.
- [14] S. Wolf, O. Eiberger, G. Hirzinger, The DLR FSJ: Energy based design of a variable stiffness joint, Proceedings of the IEEE International Conference on Robotics and Automation (ICRA) 1 (2011) 5082–5089. doi:10.1109/ICRA.2011.5980303.
- [15] A. Jafari, N. G. Tsagarakis, B. Vanderborght, D. G. Caldwell, A novel actuator with adjustable stiffness (AwAS), Proceedings of the IEEE/RSJ international conference on Intelligent robots and systems (IROS) 1 (2010) 4201–4206. doi:10.1109/IROS.2010.5648902.
- [16] B. Vanderborght, B. Verrelst, R. Van Ham, M. Van Damme, D. Lefeber, B. M. Y. Duran, P. Beyl, Exploiting natural dynamics to reduce energy consumption by controlling the compliance of soft actuators, The International Journal of Robotics Research 25 (4) (2006) 343–358. doi:10.1177/0278364906064566.
- [17] H. Q. Vu, X. Yu, F. Iida, R. Pfeifer, Improving energy efficiency of hopping locomotion by using a variable stiffness actuator, IEEE/ASME Transactions on Mechatronics 21 (1) (2016) 472–486. doi:10.1109/TMECH.2015.2428274.
- [18] R. Van Ham, T. G. Sugar, B. Vanderborght, K. W. Hollander, D. Lefeber, Compliant actuator designs, IEEE Robotics and Automation Magazine 16 (3) (2009) 81–94. doi:10.1109/MRA.2009.933629.

- [19] K. Isik, S. He, J. Ho, L. Sentis, Re-engineering a high performance electrical series elastic actuator for low-cost industrial applications, Actuators 6 (1) (2017) 5. doi:10.3390/act6010005.
- [20] B. Vanderborght, A. Albu-Schäffer, A. Bicchi, E. Burdet, D. G. Caldwell, R. Carloni, M. Catalano, O. Eiberger, W. Friedl, G. Ganesh, et al., Variable impedance actuators: A review, Robotics and autonomous systems 61 (12) (2013) 1601–1614. doi:10.1016/j.robot.2013.06.009.
- [21] A. Albu-Schäffer, O. Eiberger, et al., Soft robotics, IEEE Robotics & Automation Magazine 15 (3) (2008) 20–30. doi:10.1109/MRA.2008.927979.
- [22] N. L. Tagliamonte, F. Sergi, D. Accoto, G. Carpino, E. Guglielmelli, Double actuation architectures for rendering variable impedance in compliant robots: A review, Mechatronics 22 (8) (2012) 1187–1203. doi:10.1016/j.mechatronics.2012.09.011.
- [23] R. Van Ham, T. Sugar, et al., Compliant actuator designs: Review of actuators with passive adjustable compliance/controllable stiffness for robotic apllications, IEEE Robotics and Automation Magazine 16 (3) (2009) 81–94. doi:10.1109/MRA.2009.933629.
- [24] S. Wang, W. Van Dijk, H. van der Kooij, Spring uses in exoskeleton actuation design, Proceedings of the IEEE International Conference on Rehabilitation Robotics (ICORR) 1 (2011) 1–6. doi:10.1109/ICORR.2011.5975471.
- [25] G. Grioli, S. Wolf, et al., Variable stiffness actuators: The users point of view, The International Journal of Robotics Research 34 (6) (2015) 727–743. doi:10.1177/0278364914566515.
- [26] S. Wolf, G. Grioli, O. Eiberger, W. Friedl, M. Grebenstein, H. Höppner, E. Burdet, D. G. Caldwell, R. Carloni, M. G. Catalano, et al., Variable stiffness actuators: Review on design and components, IEEE/ASME Transactions on Mechatronics 21 (5) (2016) 2418–2430. doi:10.1109/TMECH. 2015.2501019.
- [27] R. Van Ham, B. Vanderborght, M. Van Damme, B. Verrelst, D. Lefeber, MACCEPA, the mechanically adjustable compliance and controllable equilibrium position actuator: Design and implementation in a biped robot,

- Robotics and Autonomous Systems 55 (10) (2007) 761–768. doi:10.1016/j.robot.2007.03.001.
- [28] S. Wolf, G. Hirzinger, A new variable stiffness design: Matching requirements of the next robot generation, Proceedings of the IEEE International Conference on Robotics and Automation (ICRA) 1 (2008) 1741–1746. doi:10.1109/ROBOT.2008.4543452.
- [29] M. Grebenstein, A. Albu-Schäffer, T. Bahls, M. Chalon, O. Eiberger, W. Friedl, R. Gruber, S. Haddadin, U. Hagn, R. Haslinger, et al., The DLR hand arm system, Proceedings of the IEEE International Conference on Robotics and Automation (ICRA) 1 (2011) 3175–3182. doi: 10.1109/ICRA.2011.5980371.
- [30] A. Jafari, N. G. Tsagarakis, D. G. Caldwell, AwAS-II: A new actuator with adjustable stiffness based on the novel principle of adaptable pivot point and variable lever ratio, Proceedings of the IEEE International Conference on Robotics and Automation (ICRA) 1 (2011) 4638–4643. doi:10.1109/ICRA.2011.5979994.
- [31] N. G. Tsagarakis, I. Sardellitti, D. G. Caldwell, A new variable stiffness actuator (CompAct-VSA): Design and modelling, Proceedings of the IEEE/RSJ International Conference on Intelligent Robots and Systems (IROS) 1 (2011) 378–383. doi:10.1109/IROS.2011.6095006.
- [32] F. Petit, W. Friedl, H. Höppner, M. Grebenstein, Analysis and synthesis of the bidirectional antagonistic variable stiffness mechanism, IEEE/ASME Transactions on Mechatronics 20 (2) (2015) 684–695. doi:10.1109/TMECH.2014.2321428.
- [33] M. G. Catalano, G. Grioli, F. Bonomo, R. Schiavi, A. Bicchi, VSA-HD: From the enumeration analysis to the prototypical implementation, Proceedings of the IEEE/RSJ International Conference on Intelligent Robots and Systems (IROS) 1 (2010) 3676–3681. doi:10.1109/IROS.2010.5649774.
- [34] M. G. Catalano, G. Grioli, M. Garabini, F. Bonomo, M. Mancini, N. Tsagarakis, A. Bicchi, VSA-CubeBot: A modular variable stiffness platform for multiple degrees of freedom robots, Proceedings of the IEEE International Conference on Robotics and Automation (ICRA) 1 (2011) 5090–5095. doi:10.1109/ICRA.2011.5980457.

- [35] M. Dežman, A. Gams, Pseudo-linear variable lever variable stiffness actuator: Design and evaluation, Proceedings of the IEEE International Conference on Advanced Intelligent Mechatronics (AIM) 1 (2017) 785–790. doi:10.1109/AIM.2017.8014113.
- [36] A. Calanca, R. Muradore, P. Fiorini, Impedance control of series elastic actuators: Passivity and acceleration-based control, Mechatronics 47 (2017) 37–48. doi:10.1016/j.mechatronics.2017.08.010.
- [37] R. Furnémont, G. Mathijssen, T. van der Hoeven, B. Brackx, D. Lefeber, B. Vanderborght, Torsion MACCEPA: A novel compact compliant actuator designed around the drive axis, Proceedings of the IEEE International Conference on Robotics and Automation (ICRA) 1 (2015) 232–237. doi: 10.1109/ICRA.2015.7139005.
- [38] P. Cherelle, V. Grosu, P. Beyl, A. Mathys, R. Van Ham, M. Van Damme, B. Vanderborght, D. Lefeber, The MACCEPA actuation system as torque actuator in the gait rehabilitation robot ALTACRO 1 (2010) 27–32. doi: 10.1109/BIOROB.2010.5627030.
- [39] B. Vanderborght, N. G. Tsagarakis, C. Semini, R. Van Ham, D. G. Caldwell, MACCEPA 2.0: Adjustable compliant actuator with stiffening characteristic for energy efficient hopping, Proceedings of the IEEE International Conference on Robotics and Automation (ICRA) 1 (2009) 544–549. doi:10.1109/ROBOT.2009.5152204.
- [40] J. F. Veneman, R. Ekkelenkamp, R. Kruidhof, F. C. van der Helm, H. van der Kooij, A series elastic-and bowden-cable-based actuation system for use as torque actuator in exoskeleton-type robots, The International Journal of Robotics Research 25 (3) (2006) 261–281. doi:10.1109/ICORR. 2005.1501150.
- [41] M. Dežman, A. Gams, Extending the workspace of the PLVL-variable stiffness actuator (accepted), Proceedings of the International Conference on Robotics in Alpe-Adria Danube Region 1 (2018) 0–0. doi:no-doi-yet.